Complex Variable Multi-phase Distribution System State Estimation Using Vectorized Code

Izudin Džafić, *Senior Member*, *IEEE*, Rabih A. Jabr, *Fellow*, *IEEE*, and Tarik Hrnjić, *Student Member*, *IEEE*

***Abstract*—With the advent of advanced energy management systems in distribution systems, there is a growing interest in rapid and reliable code for distribution system state estimation (DSSE) in large-scale systems. Fast DSSE methods employed in the industry are based on load scaling as they are well suited to the abundance of pseudo-measurements. Due to the paucity of real-time measurements in DSSE, phasor measurement units (PMUs) have been proposed as a potential solution to increase the estimation accuracy. However, load scaling methodologies are not extendable for exploiting PMUs. This paper proposes a high-performance DSSE method that can handle the PMUs together with all common measurement types in industrial DSSE. By using Wirtinger calculus, the method operates entirely in complex variables and employs the latest version of advanced vector extensions (AVX-2) to reap the maximum potential of computer processing units. The paper highlights the derivation of complex DSSE in matrix form, from which one can infer the implications on code reliability and maintenance. Numerical results are reported on large-scale multi-phase distribution systems, and they are contrasted with a publicly available code for DSSE in real variables. The simulation results show that loop unrolling in AVX-2 contributes about a two-fold increase in the solving speed.**

***Index Terms*—Iterative algorithm, least squares approximation, optimization method, distribution system, state estimation.**

I. Introduction

DISTRIBUTION system state estimation (DSSE) is gaining increasing interest from the electric energy industry due to its essential role in the energy management of smart grids. In recent times, there has been a rapid growth of advanced metering infrastructure (AMI) installations in addition to the interest in incorporating phasor measurement units (PMUs) in distribution systems. These have fueled the development of DSSE methods, despite a myriad of challenges including network unobservability, high R/X (resistance/reactance) ratio, unsymmetrical construction, and unbalanced operation. References [1]-[4] present detailed surveys that cover the development of DSSE from various aspects including the techniques, challenges, and future directions. Practical DSSE can be applied on large-scale systems using multi-phase models. According to [5], the computation time of conventional state estimation methods, e. g., those using the normal equations (NEs) and Hachtel's augmented matrix formulation, increases quadratically with the system size. In industrial applications, the load scaling method [6]-[8] is commonly employed due to its fast performance. However, while this method can process the classical supervisory control and data acquisition (SCADA) measurements and load data pseudo-measurements, it is not compatible with new requirements for handling PMUs. This paper proposes a complex variable DSSE solver that supports all features of industrial estimation, including PMU measurements. The implementation is in vectorized code, i.e., it employs loop unrolling and exploits the power of modern processors that posses single instruction multiple data (SIMD) extensions [9].

Network-based DSSE algorithms fall in two major categories: load scaling estimators and weighted least squares (WLS) estimators. Load scaling estimators primarily employ a power flow algorithm to balance loads with SCADA measurements, thus the implementation is efficient. Reference [6] proposes a new approach for current balancing, which forms the basis for further developments in load-adjustment DSSE. It is subsequently enhanced in [7] for power balancing over measurement areas, and in [8] to cater for weakly meshed networks. On the other hand, WLS estimators are conceptually similar to the optimization-based methods of transmission network state estimation. The classical WLS estimators are in two main types: node-voltage-based and branch-current-based. The node-voltage-based DSSE is the closest to the classical transmission network state estimator but extended to three-phase modeling [10]. The solution, which can account for non-solidly grounded networks [11], is usually obtained using the NE formulation. The augmented matrix WLS method, also known as Hachtel's matrix approach, avoids possible ill-conditioning in the NE formulation, which is linked to the high disparity in weights between zero-injection, SCADA, and load data pseudo-measurements. Reference [12] presents the implementation details of Hachtel's matrix approach for industrial-grade distribution network models, and [13] accounts for active net-

Manuscript received: January 18, 2020; accepted: May 19, 2020. Date of CrossCheck: May 19, 2020. Date of online publication: July 9, 2020.

I. Džafić (corresponding author) is with the Faculty of Electrical Engineering, University of Sarajevo, Zmaja od Bosne bb 71000 Sarajevo, Bosnia and Herzegovina (e-mail: idzafic@ieee.org).

R. A. Jabr is with the Department of Electrical & Computer Engineering, American University of Beirut, P. O. Box 11-0236, Riad El-Solh/Beirut 1107 2020, Lebanon (e-mail: rabih.jabr@aub.edu.lb).

T. Hrnjić is with the Faculty of Electrical Engineering, University of Sarajevo, Zmaja od Bosne bb 71000 Sarajevo, Bosnia and Herzegovina (e-mail: thrnjic00@gmail.com).

DOI: 10.35833/MPCE.2020.000033

works with detailed distributed generator models. Some implementations that also employ Hachtel's matrix are specialized for large-scale radial networks [14]. The branch-current-based DSSE results in decoupled per-phase estimation when all loads are Y-connected [15], [16], but its computation advantage is sustained only for radial networks. Other recent references discuss nonclassical estimation techniques such as Hamiltonian cycle theory algorithms for rapid solutions [17], and methods based on semidefinite programming relaxations (SDP). The SDP-based methods include power flow solutions that are coupled over consecutive time instants to exploit smart meter data [18], and a convex iteration scheme to improve the convergence to a rank-1 solution [19]. A promising research direction is the fully distributed three-phase state estimation based on the augmented Lagrangian method [20].

Many of the measurements in DSSE are practically pseudo-measurements obtained via short-term load forecasting (STLF) that takes as input a combination of historical/statistical load profiles, weather conditions, advanced metering infrastructure (AMI)/advanced meter reading (AMR) data, and previous state estimates [12]. The relationship between STLF and DSSE is depicted in Fig. 1. Different versions of STLF have been recently implemented via neural networks [21], machine learning algorithms [22], and clustering with partial least squares regression [11]. In general, the scarcity of real-time SCADA measurements may affect the convergence of classical iterative methods such as those employing the NE formulation. A possible remedy is via neural network. Shallow neural networks can learn to initialize the solver [23], while deep neural networks combined with Bayesian inference directly solve the minimum mean squared error estimation [24].

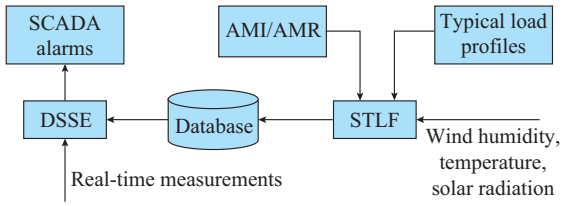

Fig. 1. Relationship between STLF and DSSE.

Reference [3] identifies the incorporation of PMU measurements in DSSE as an imminent direction for future research. Reference [25] exploits PMU measurements in DSSE to combat the SCADA measurement paucity and reliance on STLF. Other works postulate DSSE solutions within futuristic networks containing only PMU measurements [26], [27], which lead to entirely linear models. PMU measurements are, however, incompatible with some of the DSSE methods adopted by the industry such as those based on load scaling [6]-[8]. This paper proposes a wholly revamped equality-constrained WLS method for DSSE operating entirely in the complex domain. The method handles PMU measurements effectively together with the legacy type DSSE measurements and all features of industrial based DSSE. The WLS solution in complex variables is obtained via Wirtinger calculus [28], [29], which yields a distinctly elegant derivation compared to real variable solutions. The compactness of the complex matrix expressions is translated into a computer code that is easily readable, and therefore, more compliant to maintenance and upgrades. More importantly, the framework of complex variable solution is naturally suited to the implementation on modern processors that support single instruction multiple data (SIMD) operations [9], e.g., the fused multiply-accumulate complex variable operations. The DSSE solver in this article is implemented using advanced vector extensions (AVX-2) [30], which benefits from the latest version of code vectorization. The use of Wirtinger calculus has been recently gaining popularity in applications of power flow computation, as the underlying variables are naturally complex-valued. The applications are mainly in power flow [31] - [35] and transmission network state estimation [36]. The paper describes the formulation of multi-phase DSSE in the complex domain for the first time, and unravels the advantages of loop unrolling in its computer implementation. References [33], [36], [37] introduce the Wirtinger calculus and its features that are relevant to power flow modeling in positive sequence networks.

Reference [37] presents an equality-constrained hybrid state estimator in complex variables for transmission systems that are represented by their positive sequence networks. This paper extends [37] to multi-phase distribution systems with Y/Δ-connected loads and the detailed modeling of components such as the line-drop compensator. The paper contributes new vector derivative expressions that result in a compact formulation. These expressions bring the multi-phase DSSE to the level of single-phase DDSE in terms of elegance and simplicity of implementation. The use of complex variables in DSSE allows to reap the maximum potential of computer processing units by employing the latest version of AVX-2. The two primary essential aspects of DSSE include speed and accuracy. The proposed method satisfies the requirements of both speed and accuracy. Numerical results show that the real variable DSSE implementation [12] requires around double the time as compared to the complex variable implementation. The real variable formulation in [12] is not ideally suited to handle phasor measurements, as the complex measurements result in cumbersome expressions, and [12] does not present the details for dealing with phasor measurements. However, the code in [12] has been extended for a comparison with the cases with PMU measurements.

The rest of this paper is organized as follows. Section II describes the use of Wirtinger calculus for the equality-constrained WLS solution. Section III presents the three-phase modeling for DSSE in complex variables. Numerical results are reported in Section IV on multi-phase networks of 1, 2, or 3 phases, each with up to 3000 nodes. A numerical comparison of performance with [12] is also given. The paper is concluded in Section V.

II. Complex Equality-constrained DSSE

The DSSE problem in complex variables seeks to find the solution to the state vector $\boldsymbol{x}$ for a network having the following measurement equations:

$$\boldsymbol{h}(\boldsymbol{x},\bar{\boldsymbol{x}}) \approx \boldsymbol{z} \tag{1}$$

In (1), the state vector $\boldsymbol{x}$ and its conjugate $\bar{\boldsymbol{x}}$ contain three

sets of variables as follows:

1) The complex nodal voltage phasors U_K^a, U_K^b, and U_K^c for each three-phase node K. The corresponding node voltages are omitted at nodes with less than three phases.

2) The complex power absorbed in each phase of a three-phase Δ-connected load at node K: S_K^{ab}, S_K^{bc}, and S_K^{ca}.

3) The tap values of the transformer load tap changers (LTCs) are automatically controlled by their line drop compensators. Each LTC in branch KL has three tap values: t_{KL}^a, t_{KL}^b, and t_{KL}^c.

The vector of measurement functions $\boldsymbol{h}(\boldsymbol{x},\bar{\boldsymbol{x}})$ and their corresponding measurement values $\boldsymbol{z}$ are partitioned as:

$$\begin{cases} \boldsymbol{h}(\boldsymbol{x},\bar{\boldsymbol{x}}) = \begin{bmatrix} \boldsymbol{h}_c(\boldsymbol{x},\bar{\boldsymbol{x}}) \\ \bar{\boldsymbol{h}}_c(\boldsymbol{x},\bar{\boldsymbol{x}}) \\ \boldsymbol{h}_r(\boldsymbol{x},\bar{\boldsymbol{x}}) \end{bmatrix} \\ \boldsymbol{z} = \begin{bmatrix} \boldsymbol{z}_c \\ \bar{\boldsymbol{z}}_c \\ \boldsymbol{z}_r \end{bmatrix} \end{cases} \tag{2}$$

where $\boldsymbol{h}_c(\boldsymbol{x},\bar{\boldsymbol{x}})$ is a vector of complex-valued measurement functions; $\bar{\boldsymbol{h}}_c(\boldsymbol{x},\bar{\boldsymbol{x}})$ is the conjugate of $\boldsymbol{h}_c(\boldsymbol{x},\bar{\boldsymbol{x}})$; $\boldsymbol{h}_r(\boldsymbol{x},\bar{\boldsymbol{x}})$ is the vector of real-valued measurement functions; and $\boldsymbol{z}_c$, $\bar{\boldsymbol{z}}_c$, and $\boldsymbol{z}_r$ are the corresponding measurement values. Tables I and II summarize the usual complex and real measurements in DSSE.

TABLE I
COMPLEX-VALUED MEASUREMENT VECTORS

Measurement	Type	Equation
Nodal voltage phasor	PMU	(9)
Branch current phasor	PMU	(11)
Current injection phasor	PMU	(14)
Complex branch power flow	SCADA	(16)
Complex power injection from three-phase Y-connection	PSEUDO	(18)
Complex power for a three-phase Δ-connected load	PSEUDO	(19)
Complex power for a single-phase line-to-line load	PSEUDO	(29)
Zero injection node	VIRT	(14)
Three-phase Δ-connected load equation	VIRT	(23)-(25)
Single-phase line-to-line load equation	VIRT	(30)

TABLE II
REAL-VALUED MEASUREMENT VECTORS

Measurement	Type	Equation
Nodal voltage magnitude	SCADA	(33)
Line-to-line voltage magnitude	SCADA	(35)
Branch current magnitude	SCADA	(38)
Line drop compensator equation	VIRT	(41), (42)

Each table includes the corresponding equation numbers from the upcoming section in addition to one of the four common classification-based measurement types: ① PMU; ② SCADA, i.e., a real-time legacy measurement; ③ PSEUDO, i.e., a pseudo-measurement obtained via STLF; and ④ VIRT, i.e., a virtual measurement that represents a value known with certainty such as a zero injection at a node with no generation or load. Each measurement has a corresponding weight that reflects the confidence in its value, with higher weights placed on measurements that are expected to be more accurate. The virtual measurements are excluded from (1) and modeled as exact equality constraints with complex conjugate pairs and real-valued measurements:

$$\boldsymbol{c}(\boldsymbol{x},\bar{\boldsymbol{x}}) = \begin{bmatrix} \boldsymbol{c}_c(\boldsymbol{x},\bar{\boldsymbol{x}}) \\ \bar{\boldsymbol{c}}_c(\boldsymbol{x},\bar{\boldsymbol{x}}) \\ \boldsymbol{c}_r(\boldsymbol{x},\bar{\boldsymbol{x}}) \end{bmatrix} = \boldsymbol{0} \tag{3}$$

A. WLS Algorithm

The inputs of DSSE problem are the multi-phase model of the network, the measurement values in $\boldsymbol{z}$, the measurement weights placed on the diagonal of the matrix $\boldsymbol{w}$, and a termination tolerance ε. Reference [37] presents the following WLS algorithm for the solution of general state estimation problems in complex variables:

Step 1: form the expressions in the vector of measurement functions $\boldsymbol{h}(\boldsymbol{x},\bar{\boldsymbol{x}})$, c.f. Section III-A.

Step 2: form the partial derivative expressions in the Jacobian and conjugate Jacobian matrices, $\boldsymbol{H}_x$ and $\boldsymbol{H}_{\bar{x}}$, respectively, c. f. Section III-B. For m measurement functions in $\boldsymbol{h}(\boldsymbol{x},\bar{\boldsymbol{x}})$ and n state variables in $\boldsymbol{x}$, $\boldsymbol{H}_x$ and $\boldsymbol{H}_{\bar{x}}$ are given by:

$$\begin{cases} \boldsymbol{H}_x = \begin{bmatrix} \frac{\partial h_1}{\partial x_1} & \frac{\partial h_1}{\partial x_2} & \cdots & \frac{\partial h_1}{\partial x_n} \\ \frac{\partial h_2}{\partial x_1} & \frac{\partial h_2}{\partial x_2} & \cdots & \frac{\partial h_2}{\partial x_n} \\ \vdots & \vdots & & \vdots \\ \frac{\partial h_m}{\partial x_1} & \frac{\partial h_m}{\partial x_2} & \cdots & \frac{\partial h_m}{\partial x_n} \end{bmatrix} \\ \boldsymbol{H}_{\bar{x}} = \begin{bmatrix} \frac{\partial h_1}{\partial \bar{x}_1} & \frac{\partial h_1}{\partial \bar{x}_2} & \cdots & \frac{\partial h_1}{\partial \bar{x}_n} \\ \frac{\partial h_2}{\partial \bar{x}_1} & \frac{\partial h_2}{\partial \bar{x}_2} & \cdots & \frac{\partial h_2}{\partial \bar{x}_n} \\ \vdots & \vdots & & \vdots \\ \frac{\partial h_m}{\partial \bar{x}_1} & \frac{\partial h_m}{\partial \bar{x}_2} & \cdots & \frac{\partial h_m}{\partial \bar{x}_n} \end{bmatrix} \end{cases} \tag{4}$$

Similarly, the measurement functions in (3) have the Jacobian and conjugate Jacobian matrices formed by $\boldsymbol{C}_x$ and $\boldsymbol{C}_{\bar{x}}$, respectively.

Step 3: initialize the iteration counter ($k=1$) and the state vector $\boldsymbol{x}^{(1)}$.

Step 4: compute $\boldsymbol{h}\left(\boldsymbol{x}^{(k)},\bar{\boldsymbol{x}}^{(k)}\right)$, $\boldsymbol{H}^{(k)} = \left[\boldsymbol{H}_x^{(k)}, \boldsymbol{H}_{\bar{x}}^{(k)}\right]$, $\boldsymbol{c}\left(\boldsymbol{x}^{(k)},\bar{\boldsymbol{x}}^{(k)}\right)$, and $\boldsymbol{C}^{(k)} = \left[\boldsymbol{C}_x^{(k)}, \boldsymbol{C}_{\bar{x}}^{(k)}\right]$.

Step 5: compute the gain matrix $\boldsymbol{G}^{(k)}$ and the right-hand side $\boldsymbol{\beta}^{(k)}$:

$$\boldsymbol{G}^{(k)} = (\bar{\boldsymbol{H}}^{(k)})^{\mathrm{T}} \boldsymbol{W} \boldsymbol{H}^{(k)} \tag{5}$$

$$\boldsymbol{\beta}^{(k)} = \left(\bar{\boldsymbol{H}}^{(k)}\right)^{\mathrm{T}} \boldsymbol{W} \left(\boldsymbol{z} - \boldsymbol{h}\left(\boldsymbol{x}^{(k)},\bar{\boldsymbol{x}}^{(k)}\right)\right) \tag{6}$$

where $\boldsymbol{W}$ is the diagonal matrix of measurement weighting factors.

Step 6: solve the complex matrix equations using Bunch-Kaufmann decomposition:

$$\begin{bmatrix} \boldsymbol{G}^{(k)} & \left(\bar{\boldsymbol{C}}^{(k)}\right)^{\mathrm{T}} \\ \boldsymbol{C}^{(k)} & \boldsymbol{0} \end{bmatrix} \begin{bmatrix} \Delta\boldsymbol{x}^{(k)} \\ \Delta\bar{\boldsymbol{x}}^{(k)} \\ \boldsymbol{\lambda}^{(k+1)} \end{bmatrix} = \begin{bmatrix} \boldsymbol{\beta}^{(k)} \\ -\boldsymbol{c}\left(\boldsymbol{x}^{k}, \bar{\boldsymbol{x}}^{(k)}\right) \end{bmatrix} \tag{7}$$

where $\boldsymbol{\lambda}$ is a vector of Lagrangian multipliers.

Step 7: update the state vector and its conjugate:

$$\begin{bmatrix} \boldsymbol{x}^{(k+1)} \\ \bar{\boldsymbol{x}}^{(k+1)} \end{bmatrix} = \begin{bmatrix} \boldsymbol{x}^{(k)} \\ \bar{\boldsymbol{x}}^{(k)} \end{bmatrix} + \begin{bmatrix} \Delta\boldsymbol{x}^{(k)} \\ \Delta\bar{\boldsymbol{x}}^{(k)} \end{bmatrix} \tag{8}$$

Step 8: stop and print the solution if $|\Delta\boldsymbol{x}|_{\infty} < \varepsilon$. Otherwise, update the iteration counter ($k \leftarrow k+1$) and go to *Step 4*.

Figure 2 shows a flowchart of the DSSE method including bad data detection (BDD) and identification. Once bad data is detected via the chi-square test, the largest normalized residual test identifies the bad data points as described in [37]. The proposed method aims to replace the real variable implementation of DSSE, by allowing seamless handling of PMU, SCADA, virtual, and pseudo-measurements in a compact form, while the routine for dealing with bad data remains unchanged.

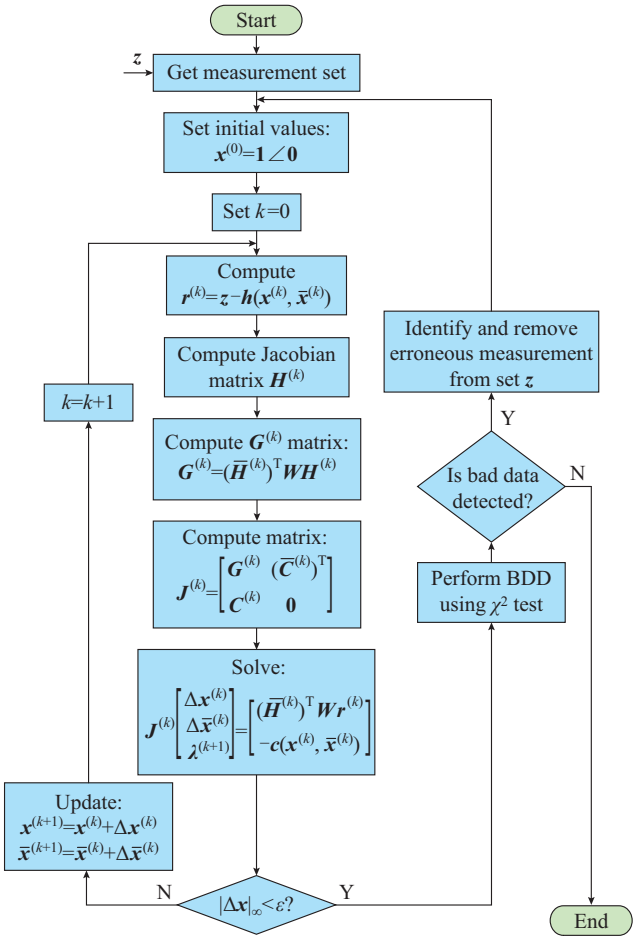

Fig. 2. Flowchart of DSSE.

B. Efficient Computation of Gain Matrix Using SIMD Optimization

The computation of the gain matrix $\boldsymbol{G}^{(k)}$ for the single-phase system is well established in the transmission network state estimation literature [38]. In the multi-phase distribution systems, it is difficult to apply the mentioned approach based on the phase; instead, the branch node model is utilized, and matrix-matrix multiplication is employed to compute the gain matrix. Matrix-matrix multiplication is best suited for SIMD optimization – basic linear algebra subprograms (BLAS) level 3 [9]. The best performance gain from SIMD optimization is obtained when the data is adjacent in memory, and conditional statements are eliminated to allow for data streaming into SIMD registers. The dimensions of the Jacobian matrix block elements depend on the number of phases of the measurement and the number of phases at the corresponding nodes.

Figures 3 and 4 show a sample network and its corresponding measurement matrix. In Fig. 4, *a*, *b* and *c* represent the three phases. The computation of the $\boldsymbol{G}_{KL}$ block element of $\boldsymbol{G}$ is determined by two factors: ① the number of phases at nodes *K* and *L* (shown by circles in Fig. 4); ② the number of phases for each measurement $\boldsymbol{M}$ where the derivatives of $\boldsymbol{M}$ with respect to the voltages $\boldsymbol{U}_K$ and $\boldsymbol{U}_L$ are nonzero (shown by the colored circles in Fig. 4, where the blue ones are input data and the red ones are the results of computation). The data in the Jacobian matrix is stored using a column-oriented approach, as indicated by the arrows in Fig. 4.

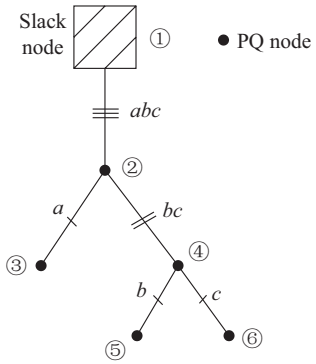

Fig. 3. Sample multi-phase network.

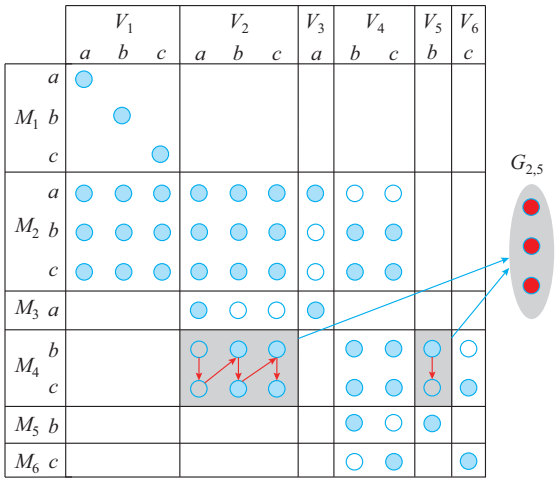

Fig. 4. Measurement Jacobian matrix.

For the implementation of efficient code, it is essential to avoid conditional statements when forming the gain matrix.

The network and the measurement set remain constant through all iterations of the DSSE algorithm, and therefore, the computation can be streamlined by checking all conditional statements at the first iteration of the algorithm and forming a list of functions. Each function contains vectorized code specific to a measurement. In subsequent iterations, the computation of the gain matrix is carried out by merely executing a call to every function in the prepared list.

III. Measurement Function Vectors and Their Partial Derivatives

Section III-A presents the complex variable formulation of the vector measurement functions in Tables I and II. The vector measurement function takes the state vector and its conjugate as input, and it gives three complex or real values if the measurement is three-phase. Given that the network is generally unsymmetrical in construction, the number of phases and consequently the size of the vector measurement function can be 1, 2, or 3. Section III-B describes how the partial derivatives of the vector functions that form the Jacobian and conjugate Jacobian matrices can be easily computed in a compact form.

A. Multi-phase Measurement Function Vectors

1) Nodal Voltage Phasor

At a three-phase node K, the nodal voltage phasor measurement function is:

$$\boldsymbol{U}_K = \begin{bmatrix} U_K^a & U_K^b & U_K^c \end{bmatrix}^{\mathrm{T}} \tag{9}$$

In general, the GPS reference can be chosen for all nodal voltage angles [39].

2) Branch Current Phasor

In a three-phase branch KL, the branch current phasors are grouped in $\boldsymbol{I}_{KL}$:

$$\boldsymbol{I}_{KL} = \begin{bmatrix} I_{KL}^a & I_{KL}^b & I_{KL}^c \end{bmatrix}^{\mathrm{T}} \tag{10}$$

The currents in (10) directed from the three-phase node K to L and the reverse currents in $\boldsymbol{I}_{LK}$ are related to the three-phase nodal voltage phasors at K and L:

$$\begin{bmatrix} \boldsymbol{I}_{KL} \\ \boldsymbol{I}_{LK} \end{bmatrix} = \begin{bmatrix} \boldsymbol{Y}_{KK} & \boldsymbol{Y}_{KL} \\ \boldsymbol{Y}_{LK} & \boldsymbol{Y}_{LL} \end{bmatrix} \begin{bmatrix} \boldsymbol{U}_K \\ \boldsymbol{U}_L \end{bmatrix} \tag{11}$$

Each sub-matrix in the nodal matrix (11), e.g., $\boldsymbol{Y}_{KL}$, is a 3×3 matrix:

$$\boldsymbol{Y}_{KL} = \begin{bmatrix} Y_{KL}^{aa} & Y_{KL}^{ab} & Y_{KL}^{ac} \\ Y_{KL}^{ba} & Y_{KL}^{bb} & Y_{KL}^{bc} \\ Y_{KL}^{ca} & Y_{KL}^{cb} & Y_{KL}^{cc} \end{bmatrix} \tag{12}$$

Note that the elements corresponding to the missing phases are omitted when a two-phase or a single-phase branch is considered.

3) Current Injection Phasor

The current injection phasors at K are grouped in $\boldsymbol{I}_K$:

$$\boldsymbol{I}_K = \begin{bmatrix} I_K^a & I_K^b & I_K^c \end{bmatrix}^{\mathrm{T}} \tag{13}$$

The measurement function is expressed in terms of the state vector via:

$$\boldsymbol{I}_K = \boldsymbol{Y}_{KK}^S \boldsymbol{U}_K + \sum_{L\in\varphi_K} \boldsymbol{Y}_{KL}^S \boldsymbol{U}_L \tag{14}$$

where $\boldsymbol{Y}_{KK}^S$ and $\boldsymbol{Y}_{KL}^S$ are 3×3 sub-matrices of the system nodal admittance matrix; and φ_K is the set of nodes connected to K by a branch.

4) Complex Branch Power Flow

The three-phase complex branch power flows from node K to L are in the vector $\boldsymbol{S}_{KL}$:

$$\boldsymbol{S}_{KL} = \begin{bmatrix} S_{KL}^a & S_{KL}^b & S_{KL}^c \end{bmatrix}^{\mathrm{T}} \tag{15}$$

The corresponding measurement function is:

$$\boldsymbol{S}_{KL} = \mathrm{diag}\left(\boldsymbol{U}_K\right)\bar{\boldsymbol{I}}_{KL} = \mathrm{diag}\left(\boldsymbol{U}_K\right)\left(\bar{\boldsymbol{Y}}_{KK}\bar{\boldsymbol{U}}_K + \bar{\boldsymbol{Y}}_{KL}\bar{\boldsymbol{U}}_L\right) \tag{16}$$

where diag(·) returns a diagonal square matrix with the elements of the argument placed on the diagonal.

5) Complex Power Injection from Three-phase Y-connection

The three-phase Y-connection with a solidly grounded neutral generally represents either the distributed generation or load, giving rise to the following complex power injection vector at K:

$$\boldsymbol{S}_K = \begin{bmatrix} S_K^a & S_K^b & S_K^c \end{bmatrix}^{\mathrm{T}} \tag{17}$$

The measurement function expresses $\boldsymbol{S}_K$ in terms of the state vector and its conjugate using the system admittance matrix blocks:

$$\boldsymbol{S}_K = \mathrm{diag}\left(\boldsymbol{U}_K\right)\bar{\boldsymbol{I}}_K = \mathrm{diag}\left(\boldsymbol{U}_K\right)\left(\bar{\boldsymbol{Y}}_{KK}^S\bar{\boldsymbol{U}}_K + \sum_{L\in\varphi_K}\bar{\boldsymbol{Y}}_{KL}^S\bar{\boldsymbol{U}}_L\right) \tag{18}$$

6) Complex Power for a Three-phase Δ-connected Load

The Δ-connected load in Fig. 5(a) is considered with the complex power phase loads that form part of the state vector:

$$\boldsymbol{S}_K^{\Delta} = \begin{bmatrix} S_K^{ab} & S_K^{bc} & S_K^{ca} \end{bmatrix} \tag{19}$$

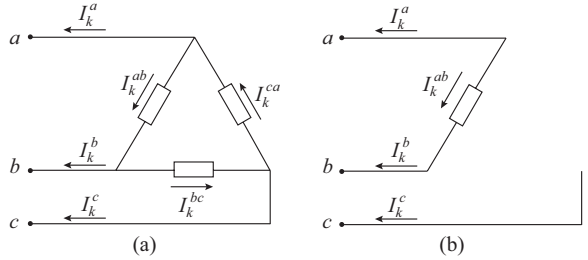

Fig. 5. Representation of difference loads. (a) Three-phase Δ-connected load. (b) Single-phase line-to-line load.

The current injections at K are:

$$I_K^a = \frac{\bar{S}_K^{ca}}{\bar{U}_K^{ca}} - \frac{\bar{S}_K^{ab}}{\bar{U}_K^{ab}} \tag{20}$$

$$I_K^b = \frac{\bar{S}_K^{ab}}{\bar{U}_K^{ab}} - \frac{\bar{S}_K^{bc}}{\bar{U}_K^{bc}} \tag{21}$$

$$I_K^c = \frac{\bar{S}_K^{bc}}{\bar{U}_K^{bc}} - \frac{\bar{S}_K^{ca}}{\bar{U}_K^{ca}} \tag{22}$$

where $U_K^{xy} = U_K^x - U_K^y,\ xy \in \{ab, bc, ca\}$. Equations (20) - (22) give rise to the following complex-valued virtual measurement equations with the injection currents computed from the network side, i.e., $\boldsymbol{I}_K$, as given by (14).

$$f_{\Delta K}^a = \bar{U}_K^{ab}\bar{U}_K^{ca} I_K^a + \bar{U}_K^{ca}\bar{S}_K^{ab} - \bar{U}_K^{ab}\bar{S}_K^{ca} = 0 \tag{23}$$

$$f_{\Delta K}^b = \bar{U}_K^{ab}\bar{U}_K^{bc} I_K^b + \bar{U}_K^{ab}\bar{S}_K^{bc} - \bar{U}_K^{bc}\bar{S}_K^{ab} = 0 \tag{24}$$

$$f_{\Delta K}^{c}=\bar{U}_{K}^{bc}\bar{U}_{K}^{ca}I_{K}^{c}+\bar{U}_{K}^{bc}\bar{S}_{K}^{ca}-\bar{U}_{K}^{ca}\bar{S}_{K}^{bc}=0 \tag{25}$$

7) Complex Power for a Single-phase Line-to-line Load

Considering the single-phase load connected between two lines as shown in Fig. 5(b), the complex power absorbed by the load is:

$$S_{K}^{ab}=\left(U_{K}^{a}-U_{K}^{b}\right)\bar{I}_{K}^{b} \tag{26}$$

In general, the complex power absorbed by the load between phase x and phase y ($xy\in\{ab,bc,ca\}$) is:

$$S_{K}^{xy}=\left(U_{K}^{x}-U_{K}^{y}\right)\bar{I}_{K}^{y}=\boldsymbol{\psi}^{xy}\boldsymbol{U}_{K}\bar{I}_{K}^{y} \tag{27}$$

where

$$\boldsymbol{\psi}^{xy}=\begin{cases}[1 & -1 & 0] & xy=ab\\ [0 & 1 & -1] & xy=bc\\ [-1 & 0 & 1] & xy=ca\end{cases} \tag{28}$$

Therefore, the measurement function is:

$$S_{K}^{xy}=\boldsymbol{\psi}^{xy}\boldsymbol{U}_{K}\left(\bar{\boldsymbol{Y}}_{KK}^{S-y}\bar{\boldsymbol{U}}_{K}+\sum_{L\in\varphi_{K}}\bar{\boldsymbol{Y}}_{KL}^{S-y}\bar{\boldsymbol{U}}_{L}\right) \tag{29}$$

where $\bar{\boldsymbol{Y}}_{KK}^{S-y}$ and $\bar{\boldsymbol{Y}}_{KL}^{S-y}$ are the rows of $\bar{\boldsymbol{Y}}_{KK}^{S}$ and $\bar{\boldsymbol{Y}}_{KL}^{S}$ corresponding to phase y, respectively. The corresponding zero sequence condition in terms of the injection currents from the network side is:

$$f_{LL}^{0}=\boldsymbol{\psi}_{0}^{xy}\boldsymbol{I}_{K}=0 \tag{30}$$

where $\boldsymbol{I}_{K}$ is given by (14) and:

$$\boldsymbol{\psi}_{0}^{xy}=\begin{cases}[1 & 1 & 0] & xy=ab\\ [0 & 1 & 1] & xy=bc\\ [1 & 0 & 1] & xy=ca\end{cases} \tag{31}$$

8) Zero Injection Node

The nodes that do not have load or generation connected to them give rise to zero injection measurements. The measurement function at K is given by (14), which is constrained to zero.

9) Nodal Voltage Magnitude

At K, the nodal voltage magnitude is:

$$\left|\boldsymbol{U}_{K}\right|=\left[\left|U_{K}^{a}\right| \quad \left|U_{K}^{b}\right| \quad \left|U_{K}^{c}\right|\right]^{\mathrm{T}} \tag{32}$$

The corresponding measurement function is:

$$\left|\boldsymbol{U}_{K}\right|=\sqrt{\mathrm{diag}\left(\bar{\boldsymbol{U}}_{K}\right)\boldsymbol{U}_{K}} \tag{33}$$

10) Line-to-line Voltage Magnitude

At K, the line-to-line voltage magnitude is:

$$\left|\boldsymbol{U}_{K}^{L}\right|=\left[\left|U_{K}^{ab}\right| \quad \left|U_{K}^{bc}\right| \quad \left|U_{K}^{ca}\right|\right]^{\mathrm{T}} \tag{34}$$

The corresponding measurement function is:

$$\left|\boldsymbol{U}_{K}^{L}\right|=\sqrt{\mathrm{diag}\left(\boldsymbol{A}_{L}\bar{\boldsymbol{U}}_{K}\right)\left(\boldsymbol{A}_{L}\boldsymbol{U}_{K}\right)} \tag{35}$$

where

$$\boldsymbol{A}_{L}=\begin{bmatrix}1 & -1 & 0\\ 0 & 1 & -1\\ -1 & 0 & 1\end{bmatrix} \tag{36}$$

11) Branch Current Magnitude

In a three-phase branch KL, the magnitudes of the branch currents are grouped in $\left|\boldsymbol{I}_{KL}\right|$:

$$\left|\boldsymbol{I}_{KL}\right|=\left[\left|I_{KL}^{a}\right| \quad \left|I_{KL}^{b}\right| \quad \left|I_{KL}^{c}\right|\right]^{\mathrm{T}} \tag{37}$$

The measurement function is:

$$\left|\boldsymbol{I}_{KL}\right|=\sqrt{\mathrm{diag}\left(\bar{\boldsymbol{I}}_{KL}\right)\boldsymbol{I}_{KL}} \tag{38}$$

12) Line Drop Compensator Equations

Consider the three-phase transformer in Fig. 6 with an LTC controlled by the line drop compensator, where K, M, and L are the node names; I_K, I_M, I_L, U_K, U_M, and U_L are the injection currents and nodal voltages of nodes K, M, and L, respectively; T is the tap value of the transformer. The tap values in the transformer in KL are part of the state vector:

$$\boldsymbol{t}_{KL}=\left[t_{KL}^{a} \quad t_{KL}^{b} \quad t_{KL}^{c}\right] \tag{39}$$

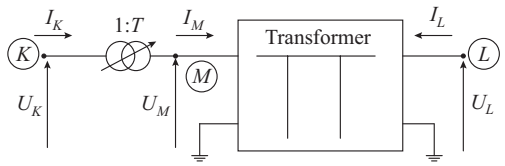

Fig. 6. Line drop compensator.

By defining $\boldsymbol{T}=\mathrm{diag}\left(\boldsymbol{t}_{KL}\right)$, the nodal matrix equation (11) for a transformer branch is generalized from the the single-phase equivalent circuit case [33]:

$$\begin{bmatrix}\boldsymbol{I}_{KL}\\ \boldsymbol{I}_{LK}\end{bmatrix}=\begin{bmatrix}\bar{\boldsymbol{T}}\boldsymbol{Y}_{MM}\boldsymbol{T} & \bar{\boldsymbol{T}}\boldsymbol{Y}_{ML}\\ \boldsymbol{Y}_{LM}\boldsymbol{T} & \boldsymbol{Y}_{LL}\end{bmatrix}\begin{bmatrix}\boldsymbol{U}_{K}\\ \boldsymbol{U}_{L}\end{bmatrix} \tag{40}$$

In the presence of a transformer with an LTC, (40) is used instead of (11) in forming the nodal admittance matrix, which makes the power and current measurement functions also dependent on $\boldsymbol{t}_{KL}$. $\boldsymbol{t}_{KL}$ is a real-valued quantity; this requirement is imposed via the following virtual measurement function:

$$\boldsymbol{f}_{t_{KL}}=\frac{\mathrm{i}}{2}\left(\bar{\boldsymbol{t}}_{KL}-\boldsymbol{t}_{KL}\right)=\boldsymbol{0} \tag{41}$$

In addition, the tap values are controlled by a line drop compensator that regulates the voltage at a target load connected to node L by a distribution line. Let $\left|\boldsymbol{U}_{ref}\right|$ denote a 3×1 vector of target voltage magnitudes and $\boldsymbol{Z}_{reg}$ denote the 3×3 compensator impedance matrix. $\boldsymbol{Z}_{reg}$ gives rise to the same per-unit voltage drop in the compensator circuit as in the actual branch where the target load is connected. Therefore, the line-drop compensator is modeled by the following additional real-valued virtual measurement vector function:

$$\boldsymbol{f}_{LDC}=\left(\boldsymbol{U}_{L}+\boldsymbol{Z}_{reg}\boldsymbol{I}_{LK}\right)\left(\bar{\boldsymbol{U}}_{L}+\bar{\boldsymbol{Z}}_{reg}\bar{\boldsymbol{I}}_{LK}\right)-\left|\boldsymbol{U}_{ref}\right|^{2}=\boldsymbol{0} \tag{42}$$

B. Partial Derivatives of Measurement Function Vectors

The majority of the above measurement functions are 3×1 vectors. It is required to compute their partial derivatives with respect to 3×1 vectors, namely $\boldsymbol{U}_K$, $\boldsymbol{S}_{KL}^{\Delta}$, $\boldsymbol{t}_{KL}$, and their conjugates. An advantage of the multi-phase complex vari-

able formulation is that the partial derivatives of the vector functions can be easily taken with respect to the quantities of vectors [40]. The computation of the partial derivatives is based on two facts described as follows.

Fact 1 Consider the vector function $\boldsymbol{y}=\boldsymbol{A}\boldsymbol{x}$, where $\boldsymbol{x}$ and $\boldsymbol{y}$ are 3×1 vectors of variables and $\boldsymbol{A}$ is a 3×3 matrix of constants. Then $\mathrm{d}\boldsymbol{y}/\mathrm{d}\boldsymbol{x}$ is a 3×3 matrix whose elements $\left(\mathrm{d}y/\mathrm{d}x\right)_{ij}=\partial y_i/\partial x_j=A_{ij}$, where $i=1,2,3$ and $j=1,2,3$, i.e.:

$$\boldsymbol{y}=\boldsymbol{A}\boldsymbol{x}\Rightarrow\frac{\mathrm{d}\boldsymbol{y}}{\mathrm{d}\boldsymbol{x}}=\boldsymbol{A} \tag{43}$$

Fact 2 Consider the vector function $\boldsymbol{y}=\boldsymbol{A}\sqrt{\boldsymbol{x}}$, where the square root function operates on each element of $\boldsymbol{x}$. Then $\mathrm{d}\boldsymbol{y}/\mathrm{d}\boldsymbol{x}$ is a 3×3 matrix with element $\left(\mathrm{d}y/\mathrm{d}x\right)_{ij}=\partial y_i/\partial x_j=A_{ij}\Big/\left(2\sqrt{x_j}\right)$, where $i=1,2,3$ and $j=1,2,3$, i.e.:

$$\boldsymbol{y}=\boldsymbol{A}\sqrt{\boldsymbol{x}}\Rightarrow\frac{\mathrm{d}\boldsymbol{y}}{\mathrm{d}\boldsymbol{x}}=\frac{1}{2}\boldsymbol{A}\mathrm{diag}\left(\boldsymbol{1}_{3\times1}\oslash\sqrt{\boldsymbol{x}}\right) \tag{44}$$

where the symbol $\oslash$ denotes the element-by-element division.

Three examples are given below to demonstrate the computation of the partial derivatives.

1) Example 1: Complex-valued Measurement Function

Consider the complex branch power flow measurement function (16), which can be written as:

$$\boldsymbol{S}_{KL}=\mathrm{diag}\left(\boldsymbol{U}_K\right)\bar{\boldsymbol{Y}}_{KK}\bar{\boldsymbol{U}}_K+\mathrm{diag}\left(\boldsymbol{U}_K\right)\bar{\boldsymbol{Y}}_{KL}\bar{\boldsymbol{U}}_L \tag{45}$$

Using (43), we can obtain:

$$\begin{cases}\dfrac{\partial\boldsymbol{S}_{KL}}{\partial\bar{\boldsymbol{U}}_K}=\mathrm{diag}\left(\boldsymbol{U}_K\right)\bar{\boldsymbol{Y}}_{KK}\\[2ex]\dfrac{\partial\boldsymbol{S}_{KL}}{\partial\bar{\boldsymbol{U}}_L}=\mathrm{diag}\left(\boldsymbol{U}_K\right)\bar{\boldsymbol{Y}}_{KL}\end{cases} \tag{46}$$

It is important to emphasize that each of the partial derivatives above is a 3×3 matrix, for instance:

$$\frac{\partial\boldsymbol{S}_{KL}}{\partial\bar{\boldsymbol{U}}_K}=\begin{bmatrix}\dfrac{\partial S_{KL}^a}{\partial\bar{U}_K^a} & \dfrac{\partial S_{KL}^a}{\partial\bar{U}_K^b} & \dfrac{\partial S_{KL}^a}{\partial\bar{U}_K^c}\\[2ex]\dfrac{\partial S_{KL}^b}{\partial\bar{U}_K^a} & \dfrac{\partial S_{KL}^b}{\partial\bar{U}_K^b} & \dfrac{\partial S_{KL}^b}{\partial\bar{U}_K^c}\\[2ex]\dfrac{\partial S_{KL}^c}{\partial\bar{U}_K^a} & \dfrac{\partial S_{KL}^c}{\partial\bar{U}_K^b} & \dfrac{\partial S_{KL}^c}{\partial\bar{U}_K^c}\end{bmatrix} \tag{47}$$

To compute the partial derivatives of $\boldsymbol{S}_{KL}$ with respect to $\boldsymbol{U}_K$ and $\boldsymbol{U}_L$, (16) is firstly re-written as:

$$\boldsymbol{S}_{KL}=\mathrm{diag}\left(\bar{\boldsymbol{I}}_{KL}\right)\boldsymbol{U}_K \tag{48}$$

Then, using (43) again, we can obtain:

$$\begin{cases}\dfrac{\partial\boldsymbol{S}_{KL}}{\partial\boldsymbol{U}_K}=\mathrm{diag}\left(\bar{\boldsymbol{I}}_{KL}\right)\\[2ex]\dfrac{\partial\boldsymbol{S}_{KL}}{\partial\boldsymbol{U}_L}=\boldsymbol{0}_{3\times3}\end{cases} \tag{49}$$

The matrix of partial derivatives for the conjugate power flow measurement vector can be deduced using the following properties for a complex-valued vector function $\boldsymbol{f}_c$ [29]:

$$\begin{cases}\dfrac{\partial\bar{\boldsymbol{f}}_c}{\partial\boldsymbol{v}}=\overline{\left(\dfrac{\partial\boldsymbol{f}_c}{\partial\bar{\boldsymbol{v}}}\right)}\\[2ex]\dfrac{\partial\bar{\boldsymbol{f}}_c}{\partial\bar{\boldsymbol{v}}}=\overline{\left(\dfrac{\partial\boldsymbol{f}_c}{\partial\boldsymbol{v}}\right)}\end{cases} \tag{50}$$

where $\boldsymbol{v}$ is a general complex variable; and $\bar{\boldsymbol{v}}$ is its conjugate.

2) Example 2: Real-valued Measurement Function

The branch current magnitude measurement function is:

$$\left|\boldsymbol{I}_{KL}\right|=\mathrm{diag}\left(\sqrt{\bar{\boldsymbol{I}}_{KL}}\right)\sqrt{\boldsymbol{I}_{KL}} \tag{51}$$

Then using the chain rule together with (44) and (11), we can obtain:

$$\frac{\partial\left|\boldsymbol{I}_{KL}\right|}{\partial\boldsymbol{U}_K}=\frac{1}{2}\mathrm{diag}\left(\sqrt{\bar{\boldsymbol{I}}_{KL}}\right)\mathrm{diag}\left(\boldsymbol{1}\oslash\sqrt{\boldsymbol{I}_{KL}}\right)\frac{\partial\boldsymbol{I}_{KL}}{\partial\boldsymbol{U}_K}=\frac{1}{2}\mathrm{diag}\left(\sqrt{\bar{\boldsymbol{I}}_{KL}\oslash\boldsymbol{I}_{KL}}\right)\boldsymbol{Y}_{KK} \tag{52}$$

$$\frac{\partial\left|\boldsymbol{I}_{KL}\right|}{\partial\boldsymbol{U}_L}=\frac{1}{2}\mathrm{diag}\left(\sqrt{\bar{\boldsymbol{I}}_{KL}\oslash\boldsymbol{I}_{KL}}\right)\boldsymbol{Y}_{KL} \tag{53}$$

For a real-valued vector function $\boldsymbol{f}_r$ such as $\left|\boldsymbol{I}_{KL}\right|$, the matrix obtained from computing the partial derivatives of $\boldsymbol{f}_r$ with respect to the conjugate variable vector is governed by the following property [29]:

$$\frac{\partial\boldsymbol{f}_r}{\partial\bar{\boldsymbol{v}}}=\overline{\left(\frac{\partial\boldsymbol{f}_r}{\partial\boldsymbol{v}}\right)} \tag{54}$$

3) Example 3: Complex-valued Measurement Function in Two Variable Types

Consider *KL* with a transformer equipped with an LTC. Based on (40), the measurement function for the phasor current on the side of *K* is:

$$\boldsymbol{I}_{KL}=\bar{\boldsymbol{T}}\boldsymbol{Y}_{MM}\boldsymbol{T}\boldsymbol{U}_K+\bar{\boldsymbol{T}}\boldsymbol{Y}_{ML}\boldsymbol{U}_L \tag{55}$$

The partial derivatives of (10) with respect to $\boldsymbol{U}_K$ and $\boldsymbol{U}_L$ can be straightforwardly computed using (43):

$$\begin{cases}\dfrac{\partial\boldsymbol{I}_{KL}}{\partial\boldsymbol{U}_K}=\bar{\boldsymbol{T}}\boldsymbol{Y}_{MM}\boldsymbol{T}\\[2ex]\dfrac{\partial\boldsymbol{I}_{KL}}{\partial\boldsymbol{U}_L}=\bar{\boldsymbol{T}}\boldsymbol{Y}_{ML}\end{cases} \tag{56}$$

To find the partial derivatives with respect to $\boldsymbol{t}_{KL}$, $\boldsymbol{T}=\mathrm{diag}\left(\boldsymbol{t}_{KL}\right)$, and (55) can be re-written as:

$$\boldsymbol{I}_{KL}=\bar{\boldsymbol{T}}\boldsymbol{Y}_{MM}\mathrm{diag}\left(\boldsymbol{U}_K\right)\boldsymbol{t}_{KL}+\bar{\boldsymbol{T}}\boldsymbol{Y}_{ML}\boldsymbol{U}_L \tag{57}$$

Then, using (43), we can obtain:

$$\frac{\partial\boldsymbol{I}_{KL}}{\partial\boldsymbol{t}_{KL}}=\bar{\boldsymbol{T}}\boldsymbol{Y}_{MM}\mathrm{diag}\left(\boldsymbol{U}_K\right) \tag{58}$$

A similar procedure yields the following equations to find the partial derivative matrix of $\boldsymbol{I}_{KL}$ with respect to $\bar{\boldsymbol{t}}_{KL}$:

$$\boldsymbol{I}_{KL} = \mathrm{diag}\left(\boldsymbol{Y}_{MM}\boldsymbol{T}\boldsymbol{U}_K\right)\bar{\boldsymbol{t}}_{KL} + \mathrm{diag}\left(\boldsymbol{Y}_{ML}\boldsymbol{U}_L\right)\bar{\boldsymbol{t}}_{KL} \Rightarrow \frac{\partial \boldsymbol{I}_{KL}}{\partial \bar{\boldsymbol{t}}_{KL}} = \mathrm{diag}\left(\boldsymbol{Y}_{MM}\boldsymbol{T}\boldsymbol{U}_K\right) + \mathrm{diag}\left(\boldsymbol{Y}_{ML}\boldsymbol{U}_L\right) \tag{59}$$

IV. Numerical Results

The proposed complex variable multi-phase distribution system state estimator (CMPhDSSE) is programmed in C++, and the computations are performed using solvers developed via the AVX-2 processor extension [30]. A comparative analysis is carried out on a multi-phase state estimator for the distribution system that uses Hachtel's matrix and operates with real variables [12]. The basic implementation is available in [41]. A Windows 10 PC with Intel i5-4690 processor and 16 GB RAM is used for numerical testing. The termination tolerance ε in Section II-A is set to be 10^{-6} per unit.

Table III shows a comparison on the IEEE 123-bus system with the measurement set in [12]. Additional phasor measurements, i.e., six PMU voltage measurements and six PMU branch current measurements, are included. The results show a snapshot of the measurement set and reveal that CMPhDSSE exhibits relative error values with respect to the true measurement values, which are generally less than those of the real variable estimator [12]. The maximum and average error values from the proposed method are less than those from [12].

TABLE III
Comparison of Estimation Results on IEEE 123-bus Test System

Node from	Node to	Measurement type	SCADA data	Reference [12]		CMPhDSSE	
				Estimated value	Error (%)	Estimated value	Error (%)
13	152	*I-a*	360.800 A	360.300	0.14	360.500	0.08
13	152	*I-b*	267.100 A	266.700	0.15	266.900	0.07
13	152	*I-c*	292.400 A	292.300	0.03	292.300	0.03
54	57	*I-a*	306.500 A	306.700	0.07	306.600	0.03
54	57	*I-b*	257.500 A	257.400	0.04	257.600	0.04
54	57	*I-c*	292.400 A	292.200	0.07	292.300	0.03
72	76	*I-a*	129.500 A	129.500	0.00	129.500	0.00
72	76	*I-b*	136.200 A	136.200	0.00	136.200	0.00
72	76	*I-c*	99.100 A	99.300	0.20	99.200	0.10
13	18	*P-abc*	1084.200 kW	1082.800	0.13	1084.500	0.03
13	18	*Q-abc*	632.400 kvar	631.500	0.14	632.800	0.06
1		*V-a*	2.292 kV	2.282	0.44	2.287	0.22
1		*V-b*	2.394 kV	2.392	0.08	2.395	0.04
1		*V-c*	2.364 kV	2.368	0.17	2.366	0.08
67		*V-ab*	3.915 kV	3.916	0.03	3.916	0.03
67		*V-bc*	4.123 kV	4.123	0.00	4.124	0.02
67		*V-ca*	4.077 kV	4.076	0.02	4.075	0.05
14		*V-a*	2.062 kV	2.074	0.58	2.066	0.19
26		*V-ca*	4.067 kV	4.061	0.15	4.069	0.05

Table IV shows a comparison of the number of iterations and the execution time on the five networks described in [12], in addition to two more extensive three-phase networks with around 1500 and 3000 nodes, respectively. The last column of Table IV represents the time ratio of [12] and CMPhDSSE. IEEE 123-bus × 2 and 123-bus × 4 networks are the IEEE 123-bus network replicated two and four times, respectively, which are described in [12].

The last two large networks are intended to model the European distribution networks that primarily have three-phase untransposed lines and unbalanced loads. Their corresponding data sets are available in [42]. The last column in Table IV shows that CMPhDSSE results in a speedup relative to [12], and the value of the speedup (1.97), which is equal to the time in [12] divided by the time of CMPhDSSE, is most substantial for the largest three-phase network. The results in Table IV are with the branch measurements (real/reactive power flow and phasor current) in the 1500-node and 3000-node three-phase networks, which correspond to 20% of the branches.

TABLE IV
Computation Performance of DSSE

Network	Reference [12]		CMPhDSSE		Improvement
	Iteration	Time (ms)	Iteration	Time (ms)	
IEEE 4-bus	2	1.4	2	1.3	1.08
IEEE 13-bus	6	13.2	6	12.4	1.06
IEEE 123-bus	4	36.1	4	32.7	1.10
IEEE 123-bus × 2	4	82.7	4	74.8	1.11
IEEE 123-bus × 4	4	104.6	4	92.7	1.13
1500-node three-phase	4	804.2	4	410.3	1.96
3000-node three-phase	4	2487.6	4	1262.6	1.97

Table V shows that increasing the proportion of branch measurements does not significantly affect the computation time.

TABLE V
EFFECT OF NUMBER OF BRANCH MEASUREMENTS ON EXECUTION TIME

Network	Percentage of branch measurements (%)	Time (ms)	Iteration
1500-node three-phase	20	410	4
	40	420	4
	60	428	4
	80	436	4
	100	444	4
3000-node three-phase	20	1262	4
	40	1498	5
	60	1529	5
	80	1577	5
	100	1598	5

V. CONCLUSION

This paper presents a vectorized implementation of equality-constrained multi-phase state estimation in complex variables. Wirtinger calculus and compact expressions of complex variable vector derivatives are the basis of the presented implementation. The underlying mathematical formulation is elegant and leads to a computer code that can be easily maintained. Additionally, the use of complex variables is ideally suited for handling the phasor measurements straightforwardly. The proposed implementation is compared with a real variable multi-phase distribution system state estimator based on Hachtel's matrix method. The basic implementation is publicly available. The comparative analysis shows that the proposed estimator has a favorable margin over the real variable Hachtel's matrix method in terms of accuracy, and is around two times faster on the three-phase distribution systems with about 3000 three-phase nodes, untransposed lines, and unbalanced loads.

REFERENCES

[1] K. Dehghanpour, Z. Wang, J. Wang *et al.*, "A survey on state estimation techniques and challenges in smart distribution systems," *IEEE Transactions on Smart Grid*, vol. 10, no. 2, pp. 2312-2322, Mar. 2019.

[2] A. Primadianto and C. Lu, "A review on distribution system state estimation," *IEEE Transactions on Power Systems*, vol. 32, no. 5, pp. 3875-3883, Sept. 2017.

[3] F. Ahmad, A. Rasool, E. Ozsoy *et al.*, "Distribution system state estimation-a step towards smart grid," *Renewable & Sustainable Energy Reviews*, vol. 81, no. 2, pp. 2659-2671, Jan. 2018.

[4] G. Wang, G. B. Giannakis, J. Chen *et al.*, "Distribution system state estimation: an overview of recent developments," *Frontiers of Information Technology & Electronics Engineering*, vol. 20, pp. 4-17, Jan. 2019.

[5] N. Nusrat, P. Lopatka, M. R. Irving *et al.*, "An overlapping zone-based state estimation method for distribution systems," *IEEE Transactions on Smart Grid*, vol. 6, no. 4, pp. 2126-2133, Jul. 2015.

[6] I. Roytelman and S. M. Shahidehpour, "State estimation for electric power distribution systems in quasi real-time conditions," *IEEE Transactions on Power Delivery*, vol. 8, no. 4, pp. 2009-2015, Oct. 1993.

[7] I. Džafić, M. Gilles, R. A. Jabr *et al.*, "Real time estimation of loads in radial and unsymmetrical three-phase distribution networks," *IEEE Transactions on Power Systems*, vol. 28, no. 4, pp. 4839-4848, Nov. 2013.

[8] I. Džafić and R. A. Jabr, "Real time multi-phase state estimation in weakly meshed distribution networks with distributed generation," *IEEE Transactions on Power Systems*, vol. 32, no. 6, pp. 4560-4569, Nov. 2017.

[9] C. J. Hughes, *Single-instruction Multiple-data Execution*. Williston: Morgan & Claypool, 2015.

[10] M. E. Baran and A. W. Kelley, "State estimation for real-time monitoring of distribution systems," *IEEE Transactions on Power Systems*, vol. 9, no. 3, pp. 1601-1609, Aug. 1994.

[11] Y. Liu, J. Li, and L. Wu, "State estimation of three-phase four-conductor distribution systems with real-time data from selective smart meters," *IEEE Transactions on Power Systems*, vol. 34, no. 4, pp. 2632-2643, Jul. 2019.

[12] I. Džafić, R. A. Jabr, I. Huseinagić *et al.*, "Multi-phase state estimation featuring industrial-grade distribution network models," *IEEE Transactions on Smart Grid*, vol. 8, no. 2, pp. 609-618, Mar. 2017.

[13] A. Ranković, B. M. Maksimović, and A. T. Sarić, "A three-phase state estimation in active distribution networks," *International Journal of Electrical Power & Energy Systems*, vol. 54, pp. 154-162, Jan. 2014.

[14] P. M. D. Jesus and A. A. R. Quintana, "Distribution system state estimation model using a reduced quasi-symmetric impedance matrix," *IEEE Transactions on Power Systems*, vol. 30, no. 6, pp. 2856-2866, Nov. 2015.

[15] M. E. Baran and A. W. Kelley, "A branch-current-based state estimation method for distribution systems," *IEEE Transactions on Power Systems*, vol. 10, no. 1, pp. 483-491, Feb. 1995.

[16] H. Wang and N. N. Schulz, "A revised branch current-based distribution system state estimation algorithm and meter placement impact," *IEEE Transactions on Power Systems*, vol. 19, no. 1, pp. 207-213, Feb. 2004.

[17] J. B. Leite and J. R. S. Mantovani, "Distribution system state estimation using the Hamiltonian cycle theory," in *Proceedings of 2016 IEEE PES General Meeting (PESGM)*, Boston, USA, Jul. 2016, pp. 1-10.

[18] S. Bhela, V. Kekatos, and S. Veeramachaneni, "Enhancing observability in distribution grids using smart meter data," *IEEE Transactions on Smart Grid*, vol. 9, no. 6, pp. 5953-5961, Nov. 2018.

[19] Y. Yao, X. Liu, D. Zhao *et al.*, "Distribution system state estimation: a semidefinite programming approach," *IEEE Transactions on Smart Grid*, vol. 10, no. 4, pp. 4369-4378, Jul. 2019.

[20] S. Chen, Z. Wei, G. Sun *et al.*, "Multi-area distributed three-phase state estimation for unbalanced active distribution networks," *Journal of Modern Power Systems and Clean Energy*, vol. 5, no. 1, pp. 767-776, Sept. 2017.

[21] E. Manitsas, R. Singh, B. C. Pal *et al.*, "Distribution system state estimation using an artificial neural network approach for pseudo measurement modeling," *IEEE Transactions on Power Systems*, vol. 27, no. 4, pp. 1888-1896, Nov. 2012.

[22] J. Wu, Y. He, and N. Jenkins, "A robust state estimator for medium voltage distribution networks," *IEEE Transactions on Power Systems*, vol. 28, no. 2, pp. 1008-1016, May 2013.

[23] A. S. Zamzam, X. Fu, and N. D. Sidiropoulos, "Data-driven learning-based optimization for distribution system state estimation," *IEEE Transactions on Power Systems*, vol. 34, no. 6, pp. 4796-4805, Nov. 2019.

[24] K. R. Mestav, J. Luengo-Rozas, and L. Tong, "Bayesian state estimation for unobservable distribution systems via deep learning," in *Proceedings of 2018 IEEE PES General Meeting (PESGM)*, Portland, USA, Aug. 2018, pp. 1-5

[25] D. A. Haughton and G. T. Heydt, "A linear state estimation formulation for smart distribution systems," *IEEE Transactions on Power Systems*, vol. 28, no. 2, pp. 1187-1195, May 2013.

[26] M. Göl and A. Abur, "A robust PMU based three-phase state estimator using modal decoupling," *IEEE Transactions on Power Systems*, vol. 29, no. 5, pp. 2292-2299, Sept. 2014.

[27] M. Majidi, M. Etezadi-Amoli, and H. Livani, "Distribution system state estimation using compressive sensing," *International Journal of Electrical Power & Energy Systems*, vol. 88, pp. 176-186, Jun. 2017.

[28] W. Wirtinger, "Zur formalen theorie der funktionen von mehr komplexen veranderlichen," *Mathematische Annalen*, vol. 97, pp. 257-376, Dec. 1927.

[29] K. Kreutz-Delgado. (2009, Jun.). The complex gradient operator and the CR-calculus. [Online]. Available: http://arXiv.org/abs/0906.4835

[30] C. Lomont. (2011, Jun.). Introduction to Intel advanced vector extensions. [Online]. Available: https://software.intel.com/en-us/articles/introduction-to-intel-advanced-vector-extensions

[31] Z. Wang, B. Cui, and J. Wang, "A necessary condition for power flow insolvability in power distribution systems with distributed genera-

tors," *IEEE Transactions on Power Systems*, vol. 32, no. 2, pp. 1440-1450, Mar. 2017.
[32] R. A. Jabr, I. Džafić, and B. C. Pal, "Compensation in complex variables for microgrid power flow," *IEEE Transactions on Power Systems*, vol. 33, no. 3, pp. 3207-3209, May 2018.
[33] I. Džafić, R. A. Jabr, and T. Hrnjić, "High performance distribution network power flow using Wirtinger calculus," *IEEE Transactions on Smart Grid*, vol. 10, no. 3, pp. 3311-3319, May 2019.
[34] J. E. Sarmiento, C. A. Alvez, B. de Nadai N. *et al.*, "A complex-valued three-phase load flow for radial networks: high-performance and low-voltage solution capability," *IEEE Transactions on Power Systems*, vol. 34, no. 4, pp. 3241-3249, Jul. 2019.
[35] R. Pires, L. Mili, and G. Chagas, "Robust complex-valued Levenberg-Marquardt algorithm as applied to power flow analysis," *International Journal of Electrical Power & Energy Systems*, vol. 113, pp. 383-392, Dec. 2019.
[36] I. Džafić, R. A. Jabr, and T. Hrnjić, "Hybrid state estimation in complex variables," *IEEE Transactions on Power Systems*, vol. 33, no. 5, Sept. 2018.
[37] I. Džafić and R. A. Jabr, "Real-time equality-constrained hybrid state estimation in complex variables," *International Journal of Electrical Power & Energy Systems*, vol. 117, May 2020.
[38] F. L. Alvarado, W. F. Tinney, and M. K. Enns, "Sparsity in large-scale network computation," in *Advances in Electric Power and Energy Conversion System Dynamics and Control.* Salt Lake City: Academic Press, 1991, pp. 1-67.
[39] A. Gómez-Expósito, A. Abur, P. Rousseaux *et al.*, "On the use of PMUs in power system state estimation," in *Proceedings of 17th Power System Computation Conference*, Stockholm, Sweden, Aug. 2011, pp. 1-13.
[40] E. Learned-Miller. (2019, Oct.). Vector, matrix, and tensor derivatives. [Online]. Available: http://cs231n.stanford.edu/vecDerivs.pdf
[41] I. Džafić, I. Huseinagić, and R. A. Jabr. (2019, Sept.). DNToolbox version 1.0.0. [Online]. Available: https://sites.google.com/site/dntoolbox/
[42] I. Džafić, R. A. Jabr, and T. Hrnjić. (2019, Oct.). Complex variable multi-phase distribution system state estimation using vectorized code – test networks. [Online]. Available: https://www.dropbox.com/s/0e0h9reasyngkfe/3ph_3kdl=0

Izudin Džafić received his Ph. D. degree from University of Zagreb, Zagreb, Croatia, in 2002. He is currently a Professor in the Department of Automatic Control and Electronics, Faculty of Electrical Engineering, at the University of Sarajevo, Sarajevo, Bosnia and Herzegovina. From 2002 to 2014, he was with Siemens AG, Nuremberg, Germany, where he held the position of the Head of the Department and Chief Product Owner (CPO) for Distribution Network Analysis (DNA) Research & Development. He is a member of the IEEE Power and Energy Society and the IEEE Computer Society. He holds 8 US and international patents. His research interests include power system modeling, development and application of fast computing to power systems simulations.

Rabih A. Jabr received the B.E. degree in electrical engineering (with high distinction) from the American University of Beirut, Beirut, Lebanon, in 1997, and the Ph.D. degree in electrical engineering from Imperial College London, London, U.K., in 2000. Currently, he is a Professor in the Department of Electrical and Computer Engineering at the American University of Beirut. His research interests include mathematical optimization techniques and power system analysis and computing.

Tarik Hrnjić received the B.Sc. and M.Sc. degrees in electrical engineering from the International University of Sarajevo, Sarajevo, Bosnia and Herzegovina, in 2015 and 2016, respectively. He is currently a Senior Assistant and Ph. D. student in the Computer Science and Informatics Department, Faculty of Electrical Engineering, University of Sarajevo. His research interests include analysis and optimization of power systems.